Black Sea Journal of Engineering and Science
doi: 10.34248/bsengineering.1850439

Open Access Journal
e-ISSN: 2619 – 8991

Research Article
Volume 9 - Issue 2: 573-584 / March 2026

IN VITRO ANTICANCER ACTIVITIES OF COMPOUNDS CONTAINING A BENZIMIDAZOLE CORE AND *IN SILICO* PHARMACOKINETIC–TOXICITY ANALYSES

Gülay DİLEK[1]*

[1]*Zonguldak Bulent Ecevit University, Faculty of Pharmacy, Department of Basic Pharmaceutical Sciences, 67600, Zonguldak, Türkiye*

Abstract: Benzimidazole-based compounds are widely recognized as versatile scaffolds in drug discovery due to their structural diversity and broad spectrum of biological activities, including anticancer effects. Breast cancer remains one of the most prevalent malignancies among women worldwide, and the high incidence, mortality rates, and emergence of resistance to current therapies highlight the need for safer and more effective treatment strategies. In this study, two different compounds containing a benzimidazole core (3a and 3b) were prepared, and the structure of the new compound (3b) was characterized using spectroscopic methods. The cytotoxic activities of 3a and 3b were comprehensively evaluated *in vitro* using two breast cancer cell lines (MCF-7 and MDA-MB-231). The results revealed concentration-dependent cytotoxic effects, with compound 3a showing higher activity against the MCF-7 cell line (IC_{50} = 88.15 µM) compared to MDA-MB-231 cells (IC_{50} = 145.80 µM). The pharmacokinetic and toxicological properties of 3a and 3b were predicted using *in silico* approaches. ADMET analyses and BOILED-Egg model results indicated that compounds 3a and 3b have good oral absorption potential and the possibility of crossing the blood-brain barrier. *In silico* toxicity assessments revealed that both compounds have an inactive profile in terms of hepatotoxicity, nephrotoxicity, and cardiotoxicity; however, they should be carefully evaluated for neurotoxicity and mutagenicity. Furthermore, based on acute oral toxicity estimates, the LD_{50} values of the compounds were calculated to be approximately 400 mg/kg, and the toxicity class was determined to be 4.

Keywords: Cytotoxic activity, Breast cancer, Benzimidazole derivatives, ProTox-II, SwissADME

***Corresponding author:** Zonguldak Bulent Ecevit University, Faculty of Pharmacy, Department of Basic Pharmaceutical Sciences, 67600, Ankara, Türkiye
E mail: gulaydilekcelik@hotmail.com (G. DİLEK)
Gülay DİLEK https://orcid.org/0000-0001-6562-2554

Received: December 27, 2025
Accepted: January 30, 2026
Published: March 15, 2026

Cite as: Dilek, G. (2026). In vitro anticancer activities of compounds containing a benzimidazole core and in silico pharmacokinetic–toxicity analyses. *Black Sea Journal of Engineering and Science*, *9*(2), 573-584.

1. Introduction

The benzimidazole core is widely used in the synthesis of numerous new molecules each year due to its ability to provide structural diversity and its pharmacophore properties. Compounds containing this ring have been reported in the literature to exhibit different biological activities, including anticancer (Kundu et al., 2025; Akkoç, 2025; Donthiboina et al., 2020), antimicrobial (Alheety et al., 2023), antifungal (Çevik et al., 2022), anti-diabetics (Naz et al., 2024), antihypertensive (Gutiérrez-Hernández et al., 2024), anti-ulcer (Cereda et al., 1987), antiparasitic (Rodríguez-Mora et al., 2024), antioxidant (Taha et al., 2024), anti-tubercular (Kızılyıldırım et al., 2025), anti-protozoal (Patel et al., 2025), and neuroprotective (Imran et al., 2021) properties. For example, Bautista-Aguilera and colleagues synthesized a new molecule containing a benzimidazole core and investigated the potential therapeutic effects of this compound for Alzheimer's disease (Bautista-Aguilera et al., 2025). There are numerous commercial drugs containing this core ingredient that are currently in clinical use. Some representative examples of these clinically approved benzimidazole-based drugs are shown in Figure 1.

Breast cancer is a malignancy that arises from uncontrolled proliferation of cells in breast tissue and is recognized as a significant public health problem on a global scale. Breast cancer is one of the most common types of malignancy among women, accounting for a significant proportion of all cancer cases. In addition, it remains a major public health issue as cancer-related mortality in women (Ferlay et al. 2021). Its association with approximately 670,000 deaths worldwide in the same year clearly demonstrates the global burden of the disease (Ferlay et al. 2021). The high incidence of breast cancer, high mortality rates, and the problem of resistance that can develop to current treatment options necessitate the development of more effective, safe, and targeted treatment approaches.

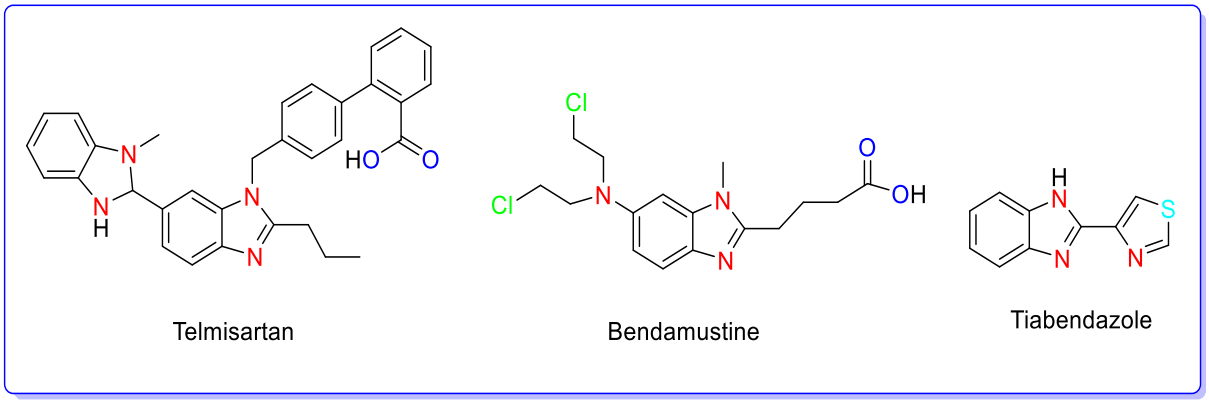

Figure 1. Biologically active drugs including benzimidazole core.

The benzimidazole core is a versatile and powerful building block in drug discovery research and holds significant potential for developing new candidate molecules for the treatment of different diseases. Therefore, the aim of this study was to synthesize two benzimidazole-based compounds, one new (3b) and one known (3a), and to evaluate their *in vitro* cytotoxic effects against breast cancer cell lines. In addition, *in silico* ADMET and BOILED-Egg model evaluations were performed to provide preliminary insights into the pharmacokinetic and safety profiles of the compounds.

2. Materials and Methods

2.1. Equipment and Supplies

All the chemicals used in the study were obtained from Sigma-Aldrich and Alfa Aesar companies and utilized without further purification. NMR spectra were recorded using a Bruker Avance III 400 spectrometer, using deuterated chloroform ($CDCl_3$) as solvents. Melting points were determined by the use of an Electrothermal Engineering IA9100 apparatus.

2.2. Synthesis of (3-Benzyl-3*H*-benzo[*d*]imidazol-5-yl)(phenyl)methanone, 3a

In the literature, it has been reported that compound **1** ((1*H*-benzo[*d*]imidazol-6-yl)(phenyl)methanone) was obtained by cyclization of (3,4-diaminophenyl)(phenyl)methanone in the presence of formic acid, and in a second step, this product was refluxed with benzyl chloride in ethyl alcohol for 8 hours to isolate compound 3a (Aktaş et al., 2025). In this study, compound 1 was commercially obtained, and the target compound was synthesized within 48 hours via a single-step reaction. For this purpose, the starting material 1 (0.50 g, 2.0 mmol) was first mixed with potassium hydroxide (0.14 g, 2.5 mmol) in ethyl alcohol (20 mL) at 25 °C for ½ h. Then, benzyl chloride (0.26 g, 2.0 mmol) was added to the reaction medium. The purified compound 3a was assessed for cytotoxic activity in cell culture studies. Yield: 82%; pale yellow solid; mp: 200–202 °C.

2.3. Synthesis of (3-(4-Methylbenzyl)-3*H*-benzo[*d*]imidazol-5-yl)(phenyl)methanone, 3b

The starting material 1 (0.50 g, 2.0 mmol), was mixed in ethyl alcohol (20 ml) in the presence of potassium hydroxide (0.14 g, 2.5 mmol) at 25 °C for 30 min. After this period, 4-methylbenzyl chloride (0.28 g, 2.0 mmol) was added to mixture, and the reaction was completed by continuing at 80 °C. At the end of the reaction period, the mixture was filtered while hot, and the resulting filtrate was left to crystallize. The product obtained by crystallization was purified and then used to evaluate its cytotoxic activity in cell culture studies. Yield: 81%; pale yellow solid; mp: 186–188 °C. ^{1}H NMR (400 MHz, $CDCl_3$, δ, ppm): 2.35 (s, 3H, $NCH_2C_6H_4(CH_3)$-4); 5.02 (s, 2H, $NCH_2C_6H_4(CH_3)$-4); 6.94-8.08 (m, 13H, Ar-*H*; NC*H*N).

2.4. Cytotoxic Activity Studies

2.4.1. Preparation of drug candidates for cell culture studies

The test substances were weighed on a precision analytical balance and fresh stock solutions were prepared in a suitable solvent. Serial dilutions were made from these stock solutions in the medium to obtain concentrations of 200, 100, 50, 25, 12.5, and 6.25 µM, and these concentrations were applied to cells in cell culture medium to perform biological effect evaluations.

2.4.2. Cell propagation and maintenance

MDA-MB-231 (human breast cancer) and HEK-293T (Human embryonic kidney) cell lines were cultured in Dulbecco's Modified Eagle Medium containing high glucose, supplemented with 10% fetal bovine serum and 1% GlutaMAX (Dilek et al., 2025). MCF-7 (human breast cancer) cells were grown in RPMI. Cells were passaged when they reached approximately 90% confluence in 25 cm^2 culture flasks. For this aim, the culture medium was first aspirated, and the cells were washed with PBS, each time with 4 mL. Then, 2.5 mL of trypsin-EDTA was added to the flask and incubated for 3 minutes. After confirming that the cells had detached from the surface under a microscope, the cell suspension was transferred to a 15 mL falcon tube. To stop the action of trypsin, 2.5 mL of culture medium was added, and the tube was centrifuged at 1450 rpm for 5 minutes. After centrifugation, the supernatant was carefully decanted and discarded, and 5 mL of medium was put to the resulting cell pellet. The cells were gently mixed with a pipette until a homogeneous suspension was obtained. To enable live

cell counting, 10 µL of trypan blue dye was added to a PCR tube, and 10 µL of the prepared cell suspension was put to the dye. After the cell-dye mixture was thoroughly homogenized, 10 µL was dropped into each well of a Thoma slide, and live-dead cell counting was performed under a light microscope.

2.4.3. Antiproliferative activity studies

Following cell counting, cells were seeded into sterile 96-well culture plates at a density of 5,000 cells per well. The plates were incubated at 37°C in a 5% CO_2 incubator for 24 hours to allow the cells to adhere to the surface. The medium in the wells was individually removed and replaced with 100 µL of fresh culture medium. The cells were exposed to compounds being tested, and the plates were again incubated for 48 h. The medium was carefully removed. 50 µL of MTT dye (5 mg/mL) was added to wells in the dark. The plates were incubated again for 2 h. After incubation, the liquid phase in the wells was carefully removed one by one using a pipette. To dissolve the formed formazan crystals, 200 µL of DMSO was added to wells, and the plates were gently shaken and incubated in the dark for 30 minutes. The plates were read using an ELISA microplate reader. The necessary calculations were performed using the absorbance values obtained, and the IC_{50} values were determined using GraphPad Prism software.

2.5. ADMET Properties

The SMILES representation of the compound 3a (O=C(C1=CC=C(N=CN2CC3=CC=CC=C3)C2=C1)C4=CC=CC=C4) and compound 3b O=C(C1=CC=C(N=CN2CC3=CC=C(C)C=C3)C2=C1)C4=CC=CC=C4 was created using ChemBioDraw Ultra 15.0 software. For this purpose, structure-based codes were used as input data for predicting pharmacokinetic behavior and toxicity properties *in silico*. While the estimation of ADME-related parameters was performed using the SwissADME online platform (Daina et al., 2017), the evaluation of toxicological profiles was carried out using the ProTox-II tool (Banerjee et al., 2018).

3. Results and Discussion

3.1. Synthesis of Compounds 3a and 3b

The targeted benzimidazole-based compounds (3a and 3b) were successfully prepared using a one-step synthesis method, as shown in Figure 2 below. Structural confirmation and characterization of 3b were performed using ^{1}H NMR spectroscopy.

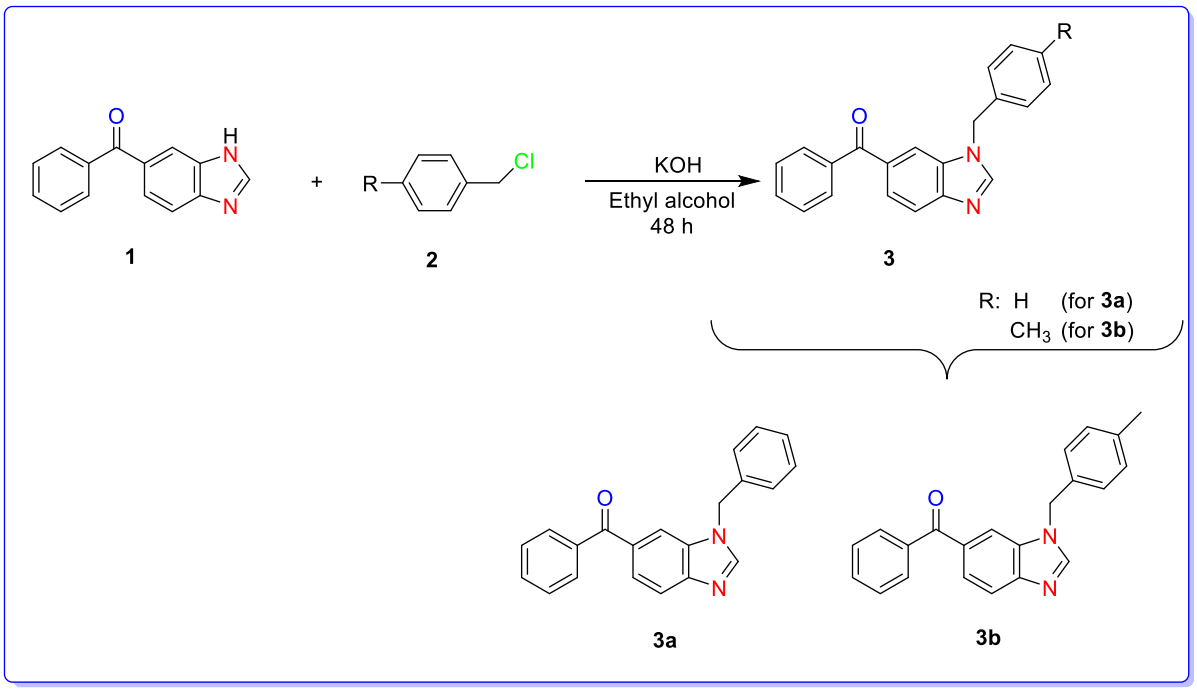

Figure 2. Synthesis route of 3a and 3b.

Upon examination of the obtained ^{1}H NMR spectra, characteristic signals indicating the successful completion of the targeted alkylation reaction were observed. Accordingly, the proton signal corresponding to the methylene (–CH_2–) group associated with the bond formed via the benzimidazole nitrogen was detected as a singlet at 5.01 ppm. Furthermore, the signal belonging to the methyl group (–CH_3) located in the para-position was observed as a singlet at 2.35 ppm, which was another important finding consistent with the structure. When these characteristic signals and all spectral data were evaluated together, it was confirmed that the synthesized compound 3b was the targeted structure (3-(4-methylbenzyl)-3*H*-benzo[*d*]imidazol-5-yl)(phenyl)methanone and that the synthesis was successfully completed.

3.2. Cytotoxic Activity Studies

The cytotoxic effects of 3a and 3b were examined in human cell lines over a 48-hour incubation period using the MTT colorimetric method. For this purpose, cells

were exposed to the compounds at different concentrations of 200, 100, 50, 25, 12.5, and 6.25 µM. The IC_{50} values obtained are presented in Table 1.

Table 1 summarizes the cytotoxic effects of compounds 3a and 3b against two breast cancer cell lines (MCF-7 and MDA-MB-231) and a healthy human embryonic kidney cell line (HEK-293T). The results obtained show that the compounds exhibit cytotoxic activity at different levels depending on the cell line.

Table 1. IC_{50} values of the tested compounds on human cell lines

Compounds	IC_{50} (µM)		
	MDA-MB-231	MCF-7	HEK-293T
3a	145.80	88.15	120.0
3b	150.50	235.3	212.70

Compound 3a had an IC_{50} value of 145.80 µM in the MDA-MB-231 cell line and 88.15 µM in the MCF-7 cell line. This result demonstrates that 3a has a higher antiproliferative effect in hormone-sensitive MCF-7 cells compared to MDA-MB-231 cells. This indicates that the mechanism of action of the compound may be influenced by cell line-specific biological differences. The IC_{50} value of the same compound in the healthy HEK-293T cell line was determined to be 120.0 µM. This value reveals that compound 3a is effective at lower concentrations against MCF-7 cells compared to healthy cells, suggesting that it exhibits a partial selectivity profile.

When compound 3b was examined, IC_{50} values of 150.50 µM and 235.30 µM were obtained in the MDA-MB-231 and MCF-7 cell lines, respectively. These results indicate that compound 3b exhibits lower cytotoxic activity in both cancer cell lines compared to 3a. The high IC_{50} value observed particularly in MCF-7 cells suggests that this cell line is more resistant to compound 3b. On the other hand, the IC_{50} value of 3b in the HEK-293T cell line was found to be 212.70 µM. This high value indicates that 3b has lower toxicity on healthy cells. However, its limited efficacy against cancer cells reveals that this compound has weaker therapeutic potential compared to compound 3a. Overall, compound 3a stands out as a more promising candidate among the compounds studied, particularly due to its lower IC_{50} value in MCF-7 cells. Figure 3 details the changes in cell viability rates resulting from the application of different concentrations of the tested compounds.

The findings reveal that the effects of the compounds on cells are concentration-dependent and that significant decreases in cell viability were observed with increasing concentrations (100 and 200 µM). While cell viability was largely preserved at low concentrations (6.25, 12.5, 25, and 50 µM), cytotoxic effects became apparent at higher concentrations, and cell proliferation was suppressed. These results indicate that the biological effects of the compounds have a dose-dependent profile.

In the literature, Akkoç (2021) synthesized a series of 1-benzyl-2-*p*-tolyl-substituted benzimidazolium salts and evaluated their cytotoxic activities against the human epithelial breast adenocarcinoma cell line (MCF-7) using the MTT assay. Among these compounds, 1-(4-methylbenzyl)-2-*p*-tolyl-1H-benzo[d]imidazole exhibited notable cytotoxic activity against MCF-7 cells with an IC_{50} value of 130 µM, which was attributed to the presence of a para-methyl substituent with electron-donating character on the phenyl ring. Similarly, Abdullah et al. (2023) reported the cytotoxic evaluation of ethyl-1-(*tert/sec*-butyl)-2-(chloro/nitrophenyl)-1*H*-benzimidazole-5-carboxylate derivatives against MCF-7 cells, identifying ethyl-1-*tert*-butyl-2-(4-chlorophenyl)-1*H*-benzimidazole-5-carboxylate as the most active compound with an IC_{50} value of 54.62 µM. In the present study, compound 3a exhibited moderate antiproliferative activity against MCF-7 cells (IC_{50} = 88.15 µM), which falls within the range reported for structurally related benzimidazole derivatives in the literature.

Considering the selectivity index (SI) values, it is observed that the selectivity profiles of 3a and 3b on breast cancer cell lines are different from each other (Table 2). For compound 3a, SI values were calculated as 0.82 in the MDA-MB-231 cell line and 0.73 in the MCF-7 cell line. These values are below 1, suggesting that compound 3a does not show significant selectivity against cancer cells in either cell line and that its cytotoxic effect may be similar to its effect on normal cells. The SI value obtained for compound 3b was 0.70 in the MDA-MB-231 cell line and 1.106 in the MCF-7 cell line. The SI value below 1 in MDA-MB-231 cells indicates low selectivity for this cell line, while the SI value above 1 calculated in MCF-7 cells reveals that compound 3b exhibits a more selective cytotoxic effect against this cell line. Overall, it can be stated that compound 3b has a more promising selectivity profile, particularly for the MCF-7 cell line, compared to compound 3a.

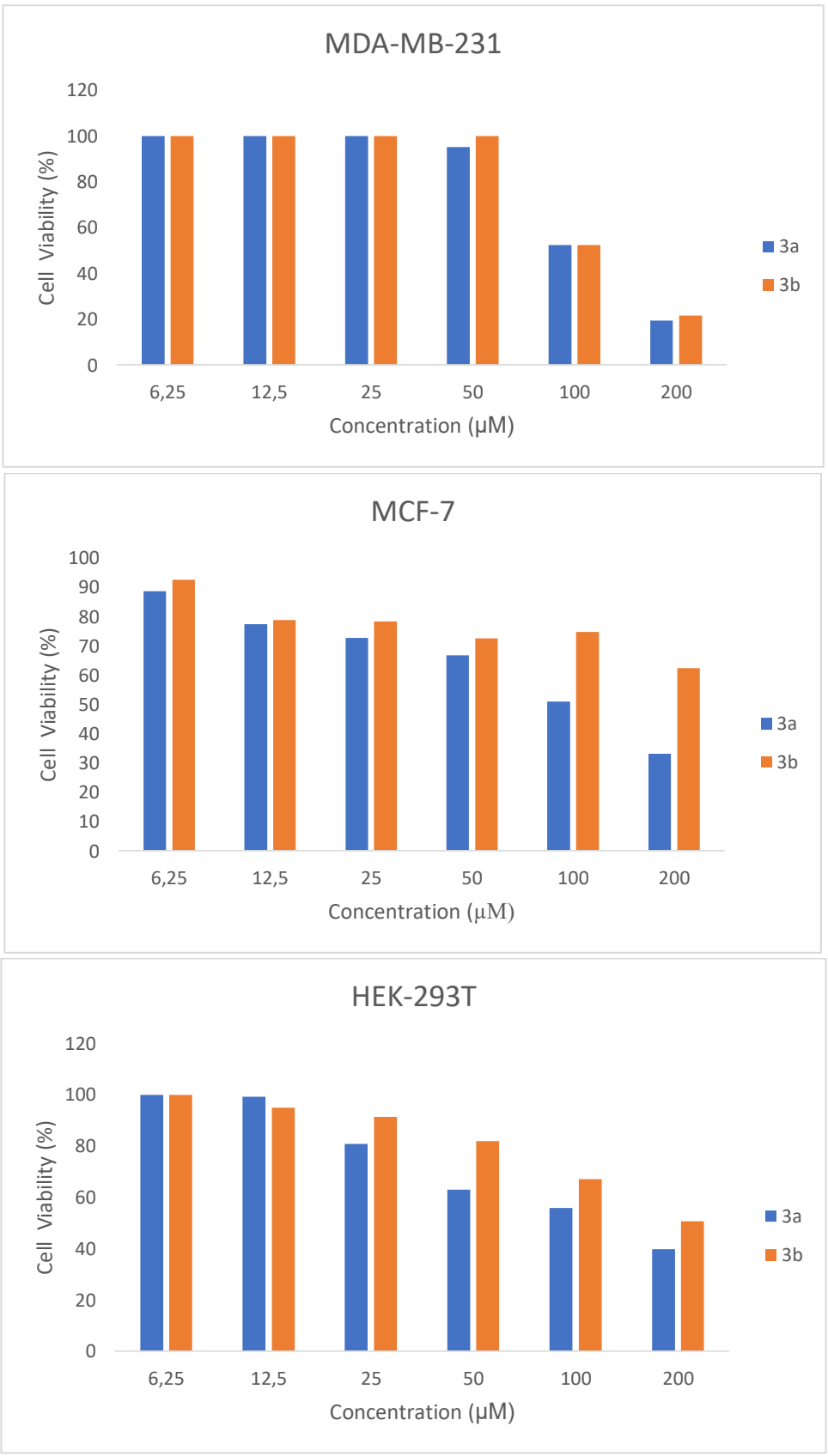

Figure 3. Cell viability ratio depends on concentrations of molecules.

Table 2. Selectivity index of compounds

Compounds	SI (IC_{50} value of HEK293T / IC_{50} value of cancer cells)		
	MDA-MB-231	MCF-7	HEK-293T
3a	0.82	0.73	1
3b	0.70	1.106	1

3.3. ADMET Properties

Akkoç (2019) investigated the *in silico* ADMET properties of a benzimidazole-based compound (1-(2-(piperidinium-1-yl)ethyl)-3-(4-vinylbenzyl)-1H-benzo[d]imidazole-3-ium dichloride) using SwissADME and ProTox-II platforms. The study reported that the compound exhibited acceptable drug-likeness characteristics, compliance with common oral bioavailability rules, and a manageable toxicity profile based on LD_{50} and toxicity class predictions. These *in silico* findings were used to support the compound's pharmacokinetic feasibility and safety profile without establishing direct experimental comparisons. In another study, the ADME properties of a 1-phenyl-3-naphthalenomethylbenzimidazolium chloride were evaluated using the SwissADME web server, with particular emphasis on physicochemical descriptors, lipophilicity, solubility, pharmacokinetic behavior, and drug-likeness rules such as Lipinski, Ghose, Veber, Egan, and Muegge (Bilici and Akkoç, 2025). The compound was reported to exhibit acceptable ADME characteristics and a moderate toxicity profile based on ProTox-II predictions, supporting its potential as a drug-like candidate. Similarly, in the present study, the ADMET properties of compounds 3a and 3b were assessed using established *in silico* tools to provide preliminary insight into their pharmacokinetic behavior and toxicity potential. The predicted parameters are intended to support the biological findings and to contextualize the synthesized compounds with respect to previously reported benzimidazole derivatives (Al-blewi et al., 2018; Husain et al., 2021; Raducka et al., 2022).

The fact that compounds 3a and 3b have an aromatic heavy atom count of 21 indicates that the structures possess a high degree of aromatic character (Table 3). The presence of four rotatable bonds suggests that the molecules have sufficient conformational flexibility, which may provide an advantage in terms of binding to the target protein. The TPSA values of 34.89 $Å^2$ for both compounds indicate a suitable polar surface area for passive diffusion through cell membranes. Furthermore, lipophilicity calculations were performed using different algorithms, and the consensus LogP values were determined to be 3.77 for 3a and 4.15 for 3b. These results indicate that compound 3b exhibits a more lipophilic character compared to compound 3a. Increased lipophilicity generally facilitates cell membrane passage but may also cause solubility issues. In this context, the higher lipophilicity of compound 3b is considered to potentially offer pharmacokinetic advantages.

The prediction of "high" gastrointestinal absorption (HIA) for both compounds is a promising finding for oral administration. Furthermore, the compounds' potential to cross the blood-brain barrier indicates that they could also be considered for central nervous system-targeted applications. Their lack of P-glycoprotein substrate properties suggests a low risk of active transport out of the cell. The skin permeability coefficients (Log Kp) for both compounds are negative and low, indicating limited but measurable skin permeability. In water solubility assessments, the compounds are classified as "moderately soluble" according to the ESOL and Ali models, while the SILICOS-IT model indicates "low solubility."

Both compounds comply with all of the Lipinski, Ghose, Veber, Egan, and Muegge rules without violation. This indicates that 3a and 3b are suitable candidates in terms of general drug-likeness. Furthermore, the bioavailability score calculated as 0.55 for both compounds supports their acceptable potential in terms of oral bioavailability. Overall, the *in silico* data for compounds 3a and 3b reveal that both structures possess potential properties for drug development. While 3b stands out with its higher lipophilicity and skin permeation potential, 3a offers a relatively more balanced lipophilicity-solubility profile.

The *in silico* toxicity predictions presented in Table 4 indicate that compounds 3a and 3b generally exhibit a similar toxicological profile at the organ level, in terms of systemic and molecular mechanisms. The prediction that both compounds are inactive in terms of hepatotoxicity, nephrotoxicity, and cardiotoxicity suggests that these compounds do not pose a significant toxic risk to vital organs. However, the active prediction of both compounds for neurotoxicity and respiratory toxicity indicates the potential presence of risks that may require careful evaluation in terms of the central nervous system and respiratory system. When toxicity extremes are evaluated, the prediction that compounds 3a and 3b are inactive in terms of carcinogenicity, immunotoxicity, and cytotoxicity stands out as a positive finding. Nevertheless, the prediction that both compounds are active in terms of mutagenicity indicates that genotoxic potential should not be overlooked. Furthermore, the active prediction of BBB (blood-brain barrier) passage suggests that these compounds may have central effects and support findings of neurotoxicity.

Table 3. *In silico* predicted some properties of 3a and 3b

Physicochemical Properties	Compounds	
	3a	3b
Molecular Formula	$C_{21}H_{16}N_2O$	$C_{22}H_{18}N_2O$
Molecular weight (MW, g/mol)	312.36	326.39
Number of heavy atoms	24	25
Number of aromatic heavy atoms (AHA)	21	21
Number of rotatable bonds (RB)	4	4
Number of H-bond acceptors (HBA)	2	2
Number of H-bond donors (HBD)	0	0
Molar Refractivity (MR)	95.36	100.32
TPSA ($Å^2$)	34.89	34.89
Lipophilicity		
Log $P_{o/w}$ (iLOGP)	2.57	3.05
Log $P_{o/w}$ (XLOGP3)	4.38	4.74
Log $P_{o/w}$ (WLOGP)	4.32	4.62
Log $P_{o/w}$ (MLOGP)	3.30	3.52
Log $P_{o/w}$ (SILICOS-IT)	4.30	4.82
Consensus Log $P_{o/w}$	3.77	4.15
Pharmacokinetics		
GI absorption	High	High
BBB permeant	Yes	Yes
P-gp substrate	No	No
CYP2C19 inhibitor	Yes	Yes
CYP3A4 inhibitor	Yes	Yes
CYP1A2 inhibitor	Yes	Yes
CYP2D6 inhibitor	Yes	Yes
CYP2C9 inhibitor	Yes	Yes
Log K_p (skin permeation, cm/s)	-5.10	-4.93
Water Solubility		
Log S (ESOL) Class	-4.92 Moderately soluble	-5.21 Moderately soluble
Log S (Ali) Class	-4.83 Moderately soluble	-5.20 Moderately soluble
Log S (SILICOS-IT) Class	-7.46 Poorly soluble	-7.83 Poorly soluble
Druglikeness		
Lipinski	Yes; 0 violation	Yes; 0 violation
Ghose	Yes	Yes
Veber	Yes	Yes
Egan	Yes	Yes
Muegge	Yes	Yes
Bioavailability score	0.55	0.55

When examined within the context of Tox21 nuclear receptor signaling pathways, the prediction that compounds 3a and 3b are inactive on hormone-related receptors such as androgen, estrogen, aromatase, and PPAR-γ indicates that the risk of endocrine-disrupting effects may be low. In evaluations based on stress response pathways and molecular initiating events, the prediction that both compounds are inactive in pathways associated with nrf2/ARE, p53, mitochondrial membrane potential, and various ion channels suggests a low likelihood of toxic effects via cellular stress and DNA damage. From a metabolic perspective, the active prediction of interactions between compounds 3a and 3b and the CYP1A2, CYP2C19, and CYP2D6 enzymes indicates that these compounds may be metabolized by certain cytochrome P450 isoenzymes. Nevertheless, their inactive prediction on CYP3A4 and CYP2E1 suggests that they may offer a relatively safer profile in terms of common drug-drug interactions (Table 4).

In silico oral toxicity predictions for compounds 3a and 3b indicate that both compounds have an LD_{50} value of approximately 400 mg/kg (Figure 4). This value suggests that the compounds exhibit moderate to low acute oral toxicity and do not pose a high risk following single-dose exposure. The predicted toxicity class 4 corresponds to the "may be harmful" category according to the Globally Harmonized System classification. This class indicates that the compounds are not highly toxic but still require careful use and dose optimization. When evaluated specifically for pharmaceutical candidates, a toxicity profile of class 4 is considered an acceptable starting point for advanced preclinical studies. The similar LD_{50} values and placement in the same toxicity class for both compounds demonstrate that their structural similarities are reflected in their toxicological behavior.

The BOILED-Egg model shown in Figure 5 enables the *in silico* evaluation of the HIA and BBB crossing potential of compounds 3a and 3b. According to the model, the positioning of both compounds within the egg diagram indicates that they possess an appropriate balance of lipophilicity and polarity to exhibit bioavailability via passive diffusion. This suggests that the compounds may have a high potential to enter systemic circulation when administered orally. In the BOILED-Egg model, the white region represents high gastrointestinal absorption, while the yellow region represents the potential to cross the BBB. When examining Figure 5, the positioning of 3a and 3b in relation to the BBB region indicates that these compounds have the potential to penetrate the central nervous system, consistent with the BBB crossing results predicted in previous *in silico* toxicity assessments and suggesting potential central effects. On the other hand, the P-glycoprotein (P-gp) substrate status in the model is also important, since compounds not subjected to active efflux may remain longer in systemic circulation and the brain. The favorable distribution profile of compounds 3a and 3b in this context can be considered an advantageous feature from a pharmacokinetic perspective. Overall, the BOILED-Egg model results indicate that compounds 3a and 3b are molecules with good oral absorption potential that can also cross the blood-brain barrier.

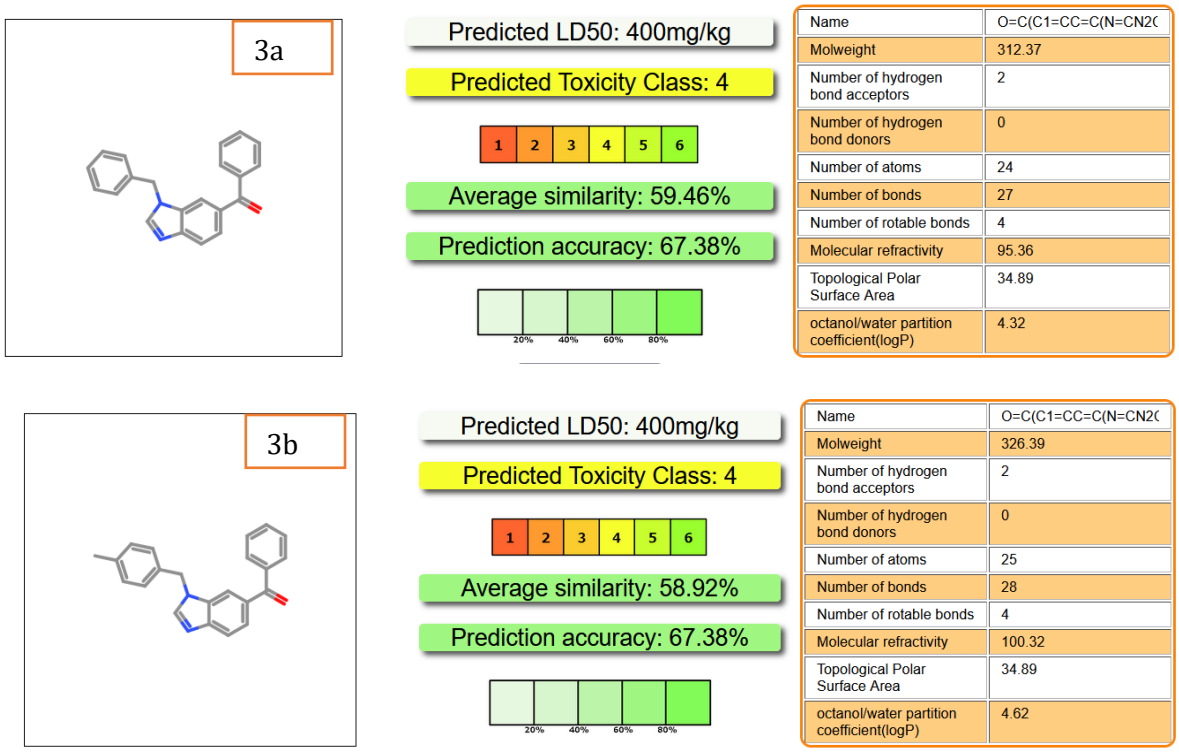

Figure 4. Oral toxicity prediction results for input compounds 3a and 3b.

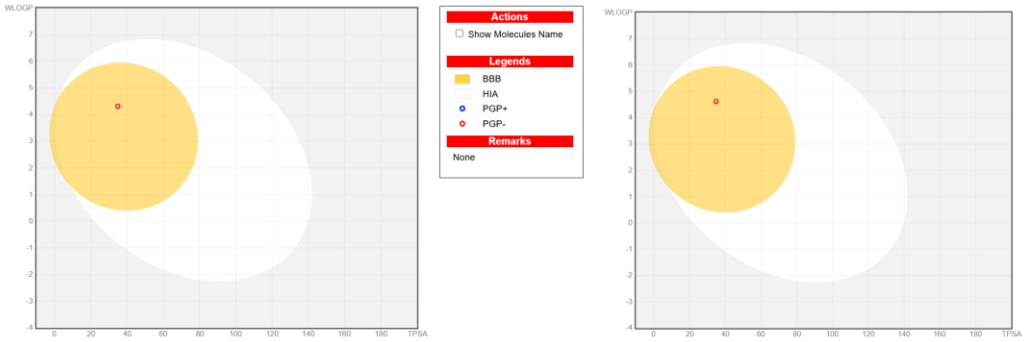

Figure 5. Boiled-egg model of compounds 3a and 3b.

4. Conclusion

In this study, two compounds (3a and 3b), one new and one known, containing a benzimidazole core were successfully synthesized, and the structure of 3b was confirmed by NMR. Cytotoxicity studies revealed that both compounds exhibited concentration-dependent antiproliferative effects on breast cancer cell lines. Especially, 3a was found to exhibit a higher antiproliferative effect in the MCF-7 cells. Moreover, compound 3b was found to exhibit a selectivity index greater than 1 against the MCF cell line. *In silico* ADMET analyses and BOILED-Egg model results showed that compounds 3a and 3b have good oral absorption potential and exhibit suitable pharmacokinetic properties. The low risk profile of both compounds in terms of hepatotoxicity, nephrotoxicity, and cardiotoxicity was considered an important advantage in terms of safety.

Table 4. *In silico* predicted organ and systemic toxicity profile of compounds 3a and 3b

Classification	Target	Prediction		Probability	
		3a	3b	3a	3b
Organ toxicity	Hepatotoxicity	Inactive	Inactive	0.83	0.84
	Neurotoxicity	Active	Active	0.92	0.90
	Nephrotoxicity	Inactive	Inactive	0.85	0.86
	Respiratory toxicity	Active	Active	0.66	0.67
	Cardiotoxicity	Inactive	Inactive	0.84	0.82
Toxicity end points	Carcinogenicity	Inactive	Inactive	0.53	0.53
	Immunotoxicity	Inactive	Inactive	0.98	0.99
	Mutagenicity	Active	Active	0.58	0.61
	Cytotoxicity	Inactive	Inactive	0.72	0.72
	BBB-barrier	Active	Active	0.94	0.93
	Ecotoxicity	Active	Active	0.76	0.75
	Clinical toxicity	Active	Active	0.55	0.54
	Nutritional toxicity	Inactive	Inactive	0.72	0.71
Tox21-Nuclear receptor signalling pathways	Aryl hydrocarbon Receptor	Inactive	Inactive	0.52	0.51
	Androgen Receptor	Inactive	Inactive	0.99	0.99
	Androgen Receptor Ligand Binding Domain	Inactive	Inactive	0.95	0.94
	Aromatase	Inactive	Inactive	0.69	0.71
	Estrogen Receptor Alpha	Inactive	Inactive	0.88	0.88
	Estrogen Receptor Ligand Binding Domain	Inactive	Inactive	0.97	0.96
	Peroxisome Proliferator Activated Receptor Gamma	Inactive	Inactive	0.97	0.97

Table 4. *In silico* predicted organ and systemic toxicity profile of compounds 3a and 3b (continuing)

Classification	Target	Prediction		Probability	
		3a	3b	3a	3b
Tox21-Stress response pathways	Nuclear factor (erythroid-derived 2)-like 2/antioxidant responsive element (nrf2/ARE)	Inactive	Inactive	0.72	0.79
	Heat shock factor response element	Inactive	Inactive	0.72	0.79
	Mitochondrial Membrane Potential	Inactive	Inactive	0.79	0.77
	Phosphoprotein (Tumor Supressor) p53	Inactive	Inactive	0.77	0.76
Molecular Initiating Events	ATPase family AAA domain-containing protein 5	Inactive	Inactive	0.95	0.95
	Thyroid hormone receptor alpha	Inactive	Inactive	0.96	0.96
	Thyroid hormone receptor beta	Inactive	Inactive	0.77	0.63
	Transtyretrin	Inactive	Inactive	0.77	0.78
	Ryanodine receptor	Inactive	Inactive	0.96	0.96
	GABA receptor	Inactive	Inactive	0.52	0.53
	Glutamate N-methyl-D-aspartate receptor	Inactive	Inactive	0.97	0.98
	alpha-amino-3-hydroxy-5-methyl-4-isoxazolepropionate receptor	Inactive	Inactive	0.99	0.99
	Kainate receptor	Inactive	Inactive	1.0	1.0
	Achetylcholinesterase	Inactive	Inactive	0.84	0.84
	Constitutive androstane receptor	Inactive	Inactive	0.99	0.99
	Pregnane X receptor	Inactive	Inactive	0.54	0.56
	NADH-quinone oxidoreductase	Inactive	Inactive	0.98	0.98
	Voltage gated sodium channel	Inactive	Inactive	0.77	0.81
	Na+/I- symporter	Inactive	Inactive	0.85	0.88
Metabolism	Cytochrome CYP1A2	Active	Active	0.67	0.68
	Cytochrome CYP2C19	Active	Active	0.61	0.59
	Cytochrome CYP2C9	Inactive	Inactive	0.52	0.54
	Cytochrome CYP2D6	Active	Active	0.71	0.72
	Cytochrome CYP3A4	Inactive	Inactive	0.56	0.53
	Cytochrome CYP2E1	Inactive	Inactive	0.90	0.93

Author Contributions

The percentages of the author contributions are presented below. The author reviewed and approved the final version of the manuscript.

	G.D.
C	100
D	100
S	100
DCP	100
DAI	100
L	100
W	100
CR	100
SR	100
PM	100

C= concept, D= design, S= supervision, DCP= data collection and/or processing, DAI= data analysis and/or interpretation, L= literature search, W= writing, CR= critical review, SR= submission and revision, PM= project management, FA= funding acquisition.

Conflict of Interest

The author declared that there is no conflict of interest.

Ethical Consideration

Ethics committee approval was not required for this study because of there was no study on animals or humans.

Acknowledgements

The author gratefully acknowledges the technical support provided by Aksen Research Laboratory for the in vitro cytotoxicity assays.

References

Abdullah, M. N., Hamid, S. A., Salhimi, S. M., Jalil, N. A. S., Al-Amin, M., & Jumali, N. S. (2023). Design and synthesis of 1-sec/tert-butyl-2-chloro/nitrophenylbenzimidazole derivatives: Molecular docking and in vitro evaluation against MDA-MB-231 and MCF-7 cell lines. *Journal of Molecular Structure*, *1277*, 134828.

Akkoç S. 2019. Derivatives of 1-(2-(piperidin-1-yl)ethyl)-1H-benzo[d]imidazole: synthesis, characterization, determining of electronic properties and cytotoxicity studies. ChemistrySelect, 4(17): 4938–4943.

Akkoç, S. (2021). Design, synthesis, characterization, and in vitro cytotoxic activity evaluation of 1,2-disubstituted benzimidazole compounds. *Journal of Physical Organic Chemistry*, *34*(4), e4125.

Akkoç, S. (2025). Antiproliferative activity, wound healing, and theoretical computational studies of compounds including the benzimidazole moiety. *Biochemical and Biophysical Research Communications*, *793*, 153006.

Aktaş, A., Özden, E. M., Celepci, D. B., Taskin-Tok, T., Ekti, F. S., Gülçin, İ., Aygün, M., Gök, Y., & Çelik, İ. (2025). 5(6)-Benzoyl-substituted benzimidazoles and their benzimidazolium salts: Design, synthesis, characterization, crystal structure, and some metabolic enzymes inhibition properties. *Archiv der Pharmazie*, *358*(7), e70063.

Al-blewi, F. F., Almehmadi, M. A., Aouad, M. R., Bardaweel, S. K., Sahu, P. K., Messali, M., Rezki, N., & El Ashry, E. S. (2018). Design, synthesis, ADME prediction and pharmacological evaluation of novel benzimidazole-1,2,3-triazole-sulfonamide hybrids as antimicrobial and antiproliferative agents. *Chemistry Central Journal*, *12*, 110.

Alheety, N. F., Mohammed, L. A., Majeed, A. H., Aydin, A., Ahmed, K. D., Alheety, M. A., Guma, M. A., & Dohare, S. (2023). Antiproliferative and antimicrobial studies of novel organic-inorganic nanohybrids of ethyl 2-((5-methoxy-1H-benzo[d]imidazol-2-yl)thio)acetate (EMBIA) with TiO2 and ZnO. *Journal of Molecular Structure*, *1274*, 134489.

Banerjee, P., Eckert, A. O., Schrey, A. K., & Preissner, R. (2018). ProTox-II: A webserver for the prediction of toxicity of chemicals. *Nucleic Acids Research*, *46*(W1), W257–W263.

Bautista-Aguilera, Ó. M., Manik, A., Diez-Iriepa, D., Szałaj, N., Zaręba, P., Więckowska, A., Żmudzki, P., Honkisz-Orzechowska, E., Knez, D., Gobec, S., Sałat, K., Martínez-Alonso, B., Guarnizo-Herrero, V., Durán, G. T., Torrado-Salmerón, C., Bellver-Sanchis, A., Nsiona-Defise, I., Ribalta-Vilella, M., Pallàs, M., López-Muñoz, F., & Iriepa, I. (2025). N-Methyl-N-((1-methyl-5-(3-(piperidin-1-yl)propoxy)-1H-benzo[d]imidazol-2-yl)methyl)prop-2-yn-1-amine (MBA-159), a new multitarget small molecule for the therapy of Alzheimer's disease. *Biomedicine & Pharmacotherapy*, *192*, 118603.

Bilici, E., & Akkoç, S. (2025). In vitro cytotoxicity in A549, Hepg2, MCF-7, and DLD-1 cancer cell lines and ADME/toxin analysis of a benzimidazole derivative. *Journal of King Saud University - Science*, *37*(2), 4242024.

Cereda, E., Turconi, M., Ezhaya, A., Bellora, E., Brambilla, A., Pagani, F., & Donetti, A. (1987). Anti-secretory and anti-ulcer activities of some new 2-(2-pyridylmethyl-sulfinyl)-benzimidazoles. *European Journal of Medicinal Chemistry*, *22*(6), 527–537.

Çevik, U. A., Celik, I., Işık, A., Pillai, R. R., Tallei, T. E., Yadav, R., Özkay, Y., & Kaplancıklı, Z. A. (2022). Synthesis, molecular modeling, quantum mechanical calculations and ADME estimation studies of benzimidazole-oxadiazole derivatives as potent antifungal agents. *Journal of Molecular Structure*, *1252*, 132095.

Daina, A., Michielin, O., & Zoete, V. (2017). SwissADME: A free web tool to evaluate pharmacokinetics, drug-likeness and medicinal chemistry friendliness of small molecules. *Scientific Reports*, *7*, 42717.

Dilek, G., Muhammed, M. T., & Akkoç, S. (2025). Synthesis, antiproliferative activity evaluation, and computational insights of benzo[d]imidazol-2(3H)-one derivatives. *ChemistrySelect*, *10*(33), e03640.

Donthiboina, K., Anchi, P., Gurram, S., Sai Mani, G., Lakshmi Uppu, J., Godugu, C., Shankaraiah, N., & Kamal, A. (2020). Synthesis and biological evaluation of substituted N-(2-(1H-benzo[d]imidazol-2-yl)phenyl)cinnamides as tubulin polymerization inhibitors. *Bioorganic Chemistry*, *103*, 104191.

Ferlay, J., Colombet, M., Soerjomataram, I., Parkin, D. M., Piñeros, M., Znaor, A., & Bray, F. (2021). Cancer statistics for the year 2020: An overview. *International Journal of Cancer*, *149*(4), 778–789.

Gutiérrez-Hernández, A., Estrada-Soto, S., Martínez-Conde, C., Gaona-Tovar, E., Medina-Franco, J. L., Hernández-Núñez, E., Hidalgo-Figueroa, S., Castro-Moreno, P., Ibarra-Barajas, M., & Navarrete-Vazquez, G. (2024). Synthesis, biosimulation and pharmacological evaluation of benzimidazole derivatives with

antihypertensive multitarget effect. *Bioorganic & Medicinal Chemistry Letters*, *110*, 129879.

Husain, A., Bhutani, M., Parveen, S., Khan, S. A., Ahmad, A., & Iqbal, M. A. (2021). Synthesis, in vitro cytotoxicity, ADME, and molecular docking studies of benzimidazole-bearing furanone derivatives. *Journal of the Chinese Chemical Society*, *68*(2), 362–373.

Imran, M., Shah, F. A., Nadeem, H., Zeb, A., Faheem, M., Naz, S., Bukhari, A., Ali, T., & Li, S. (2021). Synthesis and biological evaluation of benzimidazole derivatives as potential neuroprotective agents in an ethanol-induced rodent model. *ACS Chemical Neuroscience*, *12*(3), 489–505.

Kızılyıldırım, S., Sucu, B., Muhammed, M. T., Akkoç, S., Esatbeyoglu, T., & Ozogul, F. (2025). Experimental and theoretical studies on antituberculosis activity of different benzimidazole derivatives. *Heliyon*, *11*(4), e42674.

Kundu, S., Feizi-Dehnayebi, M., & Akkoç, S. (2025). Exploring the anticancer potential of novel benzimidazolium salts: Synthesis, biological evaluation, DFT perspective, and docking simulation for inhibition of VEGFR2. *Biochemical and Biophysical Research Communications*, *780*, 152472.

Naz, H., Othman, M. S., Rahim, F., Hussain, R., Khan, S., Taha, M., Hafez, M. M., Abdel-Hafez, L. J. M., Ullah, H., Khan, I. U., Khan, Y., & Shah, S. A. A. (2024). Investigation of novel benzimidazole-based indole/thiazole hybrids derivatives as effective anti-diabetics and anti-Alzheimer's agents: Structure–activity relationship insight, in vitro and in silico approaches. *Journal of Molecular Structure*, *1312*, 138592.

Patel, V. M., Patel, N. B., Chan-Bacab, M. J., Rivera, G., Humal, T. R., & Gamit, A. S. (2025). Synthesis and computational studies of 1,3,4-thiadiazole and benzothiazole clubbed benzimidazole analogous as anti-tubercular and anti-protozoal agent. *Journal of Molecular Structure*, *1319*, 139326.

Raducka, A., Świątkowski, M., Gobis, K., Szymański, P., & Czylkowska, A. (2022). In silico ADME and toxicity prediction of benzimidazole derivatives and its cobalt coordination compounds. Synthesis, characterization and crystal structure. *Molecules*, *27*(22), 8011.

Rodríguez-Mora, M. I., Colorado-Peralta, R., Reyes-Márquez, V., García-Eleno, M. A., Cuevas-Yáñez, E., Parra-Unda, J. R., Landa, A., & Morales-Morales, D. (2024). Effect of fluorine substituents in 4-(1-benzyl-1H-benzo[d]imidazol-2-yl)thiazole for the study of antiparasitic treatment of cysticercosis on a Taenia crassiceps model. *RSC Pharmaceutics*, *1*(5), 1055–1065.

Taha, M., Rahim, F., Adalath, B., Imran, S., Mohammed Khan, K., Adnan Ali Shah, S., Uddin, N., Nawaz, M., Bin Break, M. K., Magam, S. M., & Alqarni, S. (2024). Synthesis of benzimidazole derivatives and their antiglycation, antioxidant, antiurease and molecular docking study. *Arabian Journal of Chemistry*, *17*(4), 105700.